ELSEVIER

Advances in Water Resources 24 (2001) 49–62

Advances in Water Resources

www.elsevier.com/locate/advwatres

Numerical analysis of flow and transport in a combined heterogeneous vadose zone–groundwater system

David Russo *, Jacob Zaidel [1], Asher Laufer

Department of Environmental Physics and Irrigation, Institute of Soils, Water and Environmental Sciences, Agricultural Research Organization, The Volcani Center, Bet Dagan 50250, Israel

Received 13 April 1999; received in revised form 19 April 2000; accepted 26 April 2000

Abstract

Numerical simulations of water flow and solute transport were used to investigate the effect of the recharge (rain/irrigation) at the soil surface on solute spreading and breakthrough in a realistic, three-dimensional, heterogeneous, vadose zone–groundwater flow system. Results of the analyses suggest that smaller recharge at the soil surface increases the relative variability in the response of the unsaturated flow system, decreases the groundwater recharge from the unsaturated zone, and, concurrently, decreases the degree of nonuniformity of the groundwater flow. Consequently, smaller recharge at the soil surface enhances the longitudinal and, especially the transverse spreading of the solute plume and increases the spreading of the expected solute BTC at the lower boundary of the unsaturated zone. Furthermore, smaller recharge at the soil surface decreases the extent of the vertical penetration of the solute plume into the groundwater, slows the peak arrival of the expected BTC, and considerably increases the spreading of the expected solute BTC at a given vertical control plane in the saturated region. It was shown that for the combined flow system considered here in which the solute plume is displaced to a sufficiently large vertical distance from the inlet zone at the soil surface, the variable that controls the transport is the cumulative recharge at the soil surface, and not the recharge rate.

1. Introduction

Groundwater contamination may often originate in contamination sources which are located at or near the soil surface, such as agricultural fields, waste deposits or accidental spills. Quantitative descriptions of chemical transport in the subsurface are essential for the management of potentially hazardous chemicals with the aim of minimizing the potential of the drainage water to pollute underlying groundwater supplies. For reliability, such a description must include a realistic representation of the subsurface. The transport domain of interest in these cases is the combined vadose zone–groundwater system. Transport starts in the vadose zone, which has unique physical and chemical aspects. The vadose zone then acts as a source of water and solute for the transport processes in the saturated zone. A combined approach to solute-transport modeling is needed, which accounts for the processes unique to each of the subsystems, and at the same time properly models the mass transfer between the two subregions.

It is a common tenet nowadays that at the field scale, solute transport processes in the vadose zone as well as in the groundwater are considerably affected by the heterogeneity of the hydraulic properties of the porous formation. Natural soils exhibit a spatial heterogeneity ([27,36,46–48], among others) that is generally irregular, and is characterized by length scales which in many cases, prohibit the use of effective, or average parameters, particularly for the prediction of transport. This heterogeneity strongly affects the spatial distribution of solutes as has been observed in field experiments [5,19,39,51] and demonstrated by simulations [38,40,49,50,56] of solute transport in unsaturated, heterogeneous soils.

Similar findings concerning heterogeneity and spatial variability in aquifers have also been reported [11,26,23]. Field experiments [20,21,25,34] demonstrated the profound effect of these heterogeneities on contaminant

* Corresponding author. Tel.: +972-3-968-3866; fax: +972-3-960-4017.

E-mail address: vwrods@volcani.agri.gov.il (D. Russo).

[1] Present address: AGRA Earth & Environmental Ltd., 160 Traders Blvd. East, Suite 110, Mississauga, Ontario, Canada L4Z 3K7.

0309-1708/01/$ - see front matter
PII: S0309-1708(00)00026-9

transport and highlighted the need to account for these effects in any realistic modeling effort.

The spatial variability in formation properties and its effect on solute transport, and the paucity of measurements that are available for site characterization, has led to a concerted effort to develop theories of flow and transport based on stochastic concepts. The rationale for using stochastic concepts is that they enable media heterogeneity and data uncertainty to be treated quantitatively. Published treatments focus either on the saturated zone [8–10,12,22,35] or on the vadose zone [2,4,14,16,17,28,29,41–45,52], but very little has been done to develop an integrated modeling approach for these two subregions. For example, Destouni and Graham [18] studied solute transport through a combined soil groundwater system by using the Lagrangian approach of Dagan et al. [15]. Their approach is restricted by several simplifying assumptions regarding the statistics and the structure of the formation heterogeneity, the local flow regime and the local unsaturated conductivity. Most significantly, their approach is formulated for steady water flow, which is the exception rather than the rule in the vadose zone.

The general objective of the present study is to investigate field-scale transport in a three-dimensional (3-D), heterogeneous, combined vadose zone–groundwater flow system by means of a numerical approach. The aim is to improve our understanding of processes involved in field-scale transport in such a flow system. Specifically, the investigation will focus on the effect of the recharge (rain/irrigation) at the soil surface on the flow and the transport of a tracer solute in a vadose zone–groundwater flow system. To do so, we will combine a statistical generation method for producing realizations of heterogeneous formation properties in sufficient resolution, with an efficient numerical method for solving the partial differential equations governing flow and transport in such a flow system. The present study is a numerical experiment that provides detailed information on the consequences of the spatial heterogeneity of formation properties for the transport of solutes under realistic conditions. At the price of reduced generality, it circumvents most of the stringent assumptions of theoretical studies and facilitates analysis of simplified, yet realistic, situations at a fraction of the cost of physical experiments.

2. Theoretical considerations

2.1. Simulation of transport in a combined vadose zone–groundwater system

Our purpose here is to simulate, on the field scale, the transport of passive water-borne solutes in a combined vadose zone–groundwater flow system. We consider a 3-D flow domain that spans a considerable distance in both horizontal and vertical directions, and will analyze the transport problem by means of physically based flow and transport models and a stochastic presentation of formation properties that affect water flow and solute transport. The approach used here is a "single realization" approach [1,37,40,49,50,56], that may be understood as quantifying the macroscopic spreading of a single plume for particular site-specific applications. This spreading should be distinguished from the ensemble macrodispersive flux that accounts for differences among the trajectories of random concentration replicates over the ensemble [53]. Note that if the solute inlet zone is sufficiently large to ensure ergodicity, the discrepancy between single-realization statistics and ensemble mean statistics might be reduced significantly [13].

2.2. Governing partial differential equations

We assume here that the water flow is described locally by Richards equation, the physical parameters of which are visualized as realizations of stationary random space functions (RSFs). It is further assumed that the transport of the passive solute is described locally by a convection–dispersion equation (CDE).

In a Cartesian coordinate system (x_1, x_2, x_3), where x_1 is directed vertically downwards, assuming local isotropy and in the absence of sinks or sources, the "mixed" form of the Richards equation, governing saturated–unsaturated flow, and the CDE governing the transport of a passive solute are

$$\frac{\partial\theta}{\partial t} = \frac{\partial}{\partial x_i}\left[K\,\frac{\partial\psi}{\partial x_i}\right] - \frac{\partial K}{\partial x_1} \tag{1}$$

and

$$\frac{\partial(\theta c)}{\partial t} = \frac{\partial}{\partial x_i}\left\{\theta D_{ij}\frac{\partial c}{\partial x_j}\right\} - \frac{\partial(u_i\theta c)}{\partial x_i}, \tag{2}$$

respectively, where $i,j = 1,2,3$ and summation over repeated indices is implied in (1) and elsewhere, t is the time, $\psi = \psi(\underline{x},t)$ the pressure head, $\theta = \theta(\underline{x},t)$ the volumetric water content, $K = K(\psi,\underline{x})$ the hydraulic conductivity, c the resident solute concentration, expressed as mass per unit volume of soil solution, u_i the components of the velocity vector, and D_{ij} are the components of the pore-scale dispersion tensor. When molecular diffusion is small enough to be excluded from the analysis, D_{ij} are given [3] as

$$D_{ij} = \lambda_T|u|\delta_{ij} + (\lambda_L - \lambda_T)u_iu_j/|u|, \tag{3}$$

where λ_L and λ_T are the longitudinal and the transverse pore-scale dispersivities, δ_{ij} the Kronecker delta, and $|u| = (u_1^2 + u_2^2 + u_3^2)^{1/2}$.

Table 1
Statistical parameters of the spatially variable soil properties $\log K_s$, $\log \alpha$, n, θ_s and θ_r[a]

Parameter\soil property	$\log K_s$	$\log \alpha$	n	θ_s	θ_r
Mean, μ_p	−0.44	−0.32	2.00	0.40	0.10
Variance, σ_p^2	0.91	0.63	0.04	6×10^{-4}	4×10^{-4}
Correlation scales					
Vertical, I_{p1} (m)	0.20	0.15	0.10	0.20	0.20
Horizontal, I_{p2}, I_{p3} (m)	1.00	0.33	0.25	0.50	0.50

[a] K_s is given in m/d and α in m^{-1}.

2.3. Characterization of the flow and transport parameters

The formation hydraulic properties, characterized by the $K(\psi)$ and the $\theta(\psi)$ relationships, are hypothesized to control the field-scale solute spread. These formation properties are continuous functions of the spatial coordinates but vary in space in an irregular fashion. The length scales of these variations are much greater than the pore scale. The elementary volume (REV) representing the hydraulic properties of the heterogeneous formation is characterized by a macroscopic scale that is small in comparison with the scale of the field heterogeneities, but contains many pores. Our main concern is the effect of spatial variations of the hydraulic properties on solute transport. Therefore, deterministic, constant values were adopted for pore-scale dispersivities: $\lambda_L = 2\times10^{-3}$ m and $\lambda_T = 1\times10^{-4}$ m.

To simplify the analysis, it is assumed that the local $K(\psi)$ and $\theta(\psi)$ relationships are described by the van Genuchten [57] parametric expressions. Ignoring hysteresis and local anisotropy, and considering the pressure head, ψ, as the dependent variable, they read:

$$\Theta(\psi,\underline{x}) = \left\{\frac{1}{1+[\alpha(\underline{x})|\psi|]^{n(\underline{x})}}\right\}^{m(\underline{x})},$$

$$K(\psi,\underline{x}) = K_s(\underline{x})\frac{\left\{1-[\alpha(\underline{x})|\psi|]^{n(\underline{x})-1}\left\{1+[\alpha(\underline{x})|\psi|]^{n(\underline{x})}\right\}^{-m(\underline{x})}\right\}^2}{\left\{1+[\alpha(\underline{x})|\psi|]^{n(\underline{x})}\right\}^{m(\underline{x})/2}}, \quad (4)$$

where $\Theta = (\theta-\theta_r)/(\theta_s-\theta_r)$ is the effective water saturation, θ_s and θ_r the saturated and residual water contents, respectively, K_s the saturated conductivity, α and m the parameters which are related to the formation pore size distribution, and $n = 1/(1-m)$.

It is assumed further that each parameter in (4), denoted by $p(\underline{x})$, is a second-order stationary, statistically anisotropic random space function (RSF). They are completely characterized by a constant mean, $\langle p(\underline{x})\rangle$, which is independent of the spatial position, and a covariance, $C_{pp}(\underline{x},\underline{x}')$ that, in turn, depends on the separation vector, $\underline{\xi} = \underline{x}-\underline{x}'$ and not on $\underline{x}$ and $\underline{x}'$ individually. A 3-D, exponential covariance is adopted here for $p(\underline{x})$, i.e.

$$C_{pp}(\underline{\xi}) = \sigma_p^2 \exp[-\xi'], \quad (5)$$

where $\underline{\xi}' = (\underline{x}-\underline{x}')/\underline{I}_p$ is the scaled separation vector, $\xi' = |\underline{\xi}'|$, σ_p^2 and $\underline{I}_p = (I_{p1}, I_{p2}, I_{p3})$ are the variance and correlation scales of $p(\underline{x})$, respectively. In line with field studies [6,48,54] axisymmetric anisotropy is adopted for $C_{pp}(\underline{\xi})$. That is, $I_{pv} = I_{p1}$ and $I_{ph} = I_{p2} = I_{p3}$ are the characteristic length scales of $p(\underline{x})$ in the vertical direction, and in the horizontal plane, respectively. Statistical properties of the various formation parameters of (4) were derived from measurements in the Bet Dagan trench [46] and are summarized in Table 1.

2.4. Generation of the flow and transport parameters field

With a single realization approach, inference of statistical moments of the distribution of relevant flow-attributed variables requires a flow domain that is sufficiently large compared with the correlation scales of the pertinent formation properties. In addition, in order to preserve details of the spatial structure of the formation properties, the size of the numerical cells must be small compared with the characteristic length scale of the heterogeneity of the relevant formation properties.

We considered a flow domain of 12 m in the x_1 vertical direction, and 25 and 10 m in the x_2 and the x_3 horizontal directions, respectively. This provided a flow domain spanning 50, 25 and 10 correlation length scales of $\log K_s$ in the respective directions. Based on the criterion of at least four nodes per correlation length suggested by Ababou [1], the flow domain was discretized into a large number of equalized cells, measuring 0.05 and 0.25 m in the vertical and horizontal directions, respectively. This provided four nodes per correlation length scale of $\log K_s$, but smaller number of nodes per correlation length scale in the case of the other input formation parameters (Table 1). Note that the correlation scale of log-unsaturated conductivity, $\log K$, may be smaller than that of $\log K_s$ [29]. Consequently, the aforementioned discretization of the flow domain may not meet the criterion of four nodes per correlation length of $\log K$. This subject, however, was not addressed here and is left for future investigation.

The covariance function (5) and the values of σ_p^2, I_{ph} and I_{pv} (Table 1) were used in applying the turning bands method [55] to generate independent realizations of $\log K_s$, $\log\alpha$, n, θ_s and θ_r for each of the $100 \times 40 \times 200$ cells of the flow domain. By means of (4), 2-D tables of relative conductivity, $K^r_{\iota\ell} = K/K_s$ and relative water content, $\theta^r_{\iota\ell} = (\theta - \theta_r)/(\theta_s - \theta_r)$ were constructed as functions of $\alpha'_\iota = (\iota - 1)\delta_\alpha$ and $n_\ell = 1.1 + (\ell - 1)\delta_n$, where $\alpha' = \alpha|\psi|$, $\iota = 1$ to N_α, $\ell = 1$ to N_n, $N_\alpha = 50000$, $N_n = 80$, $\delta_\alpha = 0.01$ and $\delta_n = 0.05$. A bilinear interpolation scheme was used in applying these tables to calculate values of K^r and $\theta = \theta^r(\theta_s - \theta_r) + \theta_s$ for each cell of the flow domain by means of the generated realizations of α, n, θ_s and θ_r and the simulated water pressure head, ψ. Hydraulic conductivity between cells, the so-called interblock conductivity, was estimated from the generated realization of K_s and the calculated K^r, by means of a modified version of the asymptotic weighting (AW) scheme proposed by Zaidel and Russo [60]. In this modification, in the vicinity of the water table, the interblock relative conductivity in the vertical direction for the capillary interblock term, k^r_{z-} capillary, was approximated by its counterpart for the gravity interblock term, k^r_{z-} gravity. The latter was calculated by a modified scheme that is more accurate than the upstream weighting scheme and more stable than the arithmetic mean scheme (i.e., this scheme does not create oscillations for gravity-dominated flow).

2.5. Boundary and initial conditions

For the analyses presented here, we considered the movement of a passive solute in a flow domain, Ω, which comprised an initially solute-free porous formation with initially hydrostatic distribution of pressure heads, i.e., $\psi_i(x_1, x_2, x_3) = x_1 - \zeta(x_2, x_3)$, where $\zeta(x_2, x_3)$ is the initial depth to the water table. The mean, steady-state, groundwater flow is assumed to be unidirectional, parallel to the x_2-axis. Consequently, the water table is initially inclined from $x_2 = 0$ to $x_2 = L_2$. No flow conditions are assumed for the lower boundary of the modeling domain located at $x_1 = L_1$ (i.e., the bottom of the aquifer), and for the $x_3 = 0$ and $x_3 = L_3$ boundaries, which are parallel to the mean regional flow direction. Above the water table, no flow conditions are assumed for the $x_2 = 0$ and $x_2 = L_2$ boundaries. Below the water table, fixed pressure heads, $\psi_{bl}(l = 0, L)$ are specified along the $x_2 = 0$ and $x_2 = L_2$ boundaries. These heads are calculated on the basis of the specified depth to the water table along the vertical boundaries and the hydrostatic assumption.

Water flow in the unsaturated zone is originated from a periodic potential flux, $F(t_j)$, imposed on the entire soil surface located at $x_1 = 0$. The potential flux is given by $F(t_j) = \mathrm{RI}(x_2, x_3)$, $t'_j < t_j < t''_j$, $F(t_j) = 0$, elsewhere, where $\mathrm{RI}(x_2, x_3) > 0$ is the spatially variable rain/irrigation intensity, $j = 1$ to N_i, and N_I is the number of the irrigation/rain events. For the flow, the appropriate boundary and initial conditions are:

$$K(\psi)\frac{\partial\psi}{\partial x_1} + K(\psi) \leqslant F(t), \quad x_1 = 0, \quad 0 \leqslant x_2 \leqslant L_2, \quad 0 \leqslant x_3 \leqslant L_3, \quad t > 0, \tag{6a}$$

$$\frac{\partial\psi}{\partial x_1} = 0, \quad x_1 = L_1, \quad 0 \leqslant x_2 \leqslant L_2, \quad 0 \leqslant x_3 \leqslant L_3, \quad t > 0, \tag{6b}$$

$$-K(\psi)\frac{\partial\psi}{\partial x_2} = 0, \quad x_2 = 0, \quad x_2 = L_2, \quad 0 \leqslant x_1 \leqslant \zeta(x_2, x_3), \quad 0 \leqslant x_3 \leqslant L_3, \quad t > 0, \tag{6c}$$

$$\psi = \psi_{bl}, \quad x_2 = 0, \quad x_2 = L_2, \quad \zeta(x_2, x_3) \leqslant x_1 \leqslant L_1, \quad 0 \leqslant x_3 \leqslant L_3, \quad t > 0, \tag{6d}$$

$$-K(\psi)\frac{\partial\psi}{\partial x_3} = 0, \quad x_3 = 0, \quad x_3 = L_3, \quad 0 \leqslant x_1 \leqslant L_1, \quad 0 \leqslant x_2 \leqslant L_2, \quad t > 0, \tag{6e}$$

$$\psi = x_1 - \zeta(x_2, x_3), \quad 0 \leqslant x_1 \leqslant L_1, \quad 0 \leqslant x_2 \leqslant L_2, \quad 0 \leqslant x_3 \leqslant L_3, \quad t = 0. \tag{6f}$$

For the transport, we considered a case in which a solute with concentration, c_0, invades the soil during time, t_0 via a planar source of dimensions $(\rho_{22} - \rho_{21}) \times (\rho_{32} - \rho_{31})$ located at the soil surface ($x_1 = 0$), which is orthogonal to the vertical mean flow direction. There is no solute transport across the soil surface outside the source, nor across the vertical planes located at $x_2 = 0$ and $x_2 = L_2$ above the water table, nor across the vertical planes located at $x_3 = 0$ and $x_3 = L_3$, for which the normal derivatives of c vanish. A zero-gradient-boundary is also specified at the bottom ($x_1 = L_1$). Note that the solute flux across the vertical planes located at $x_2 = 0$ and $x_2 = L_2$ below the water table does not vanish because of the convective flux of the solute, $u_2\theta c (u_2 \neq 0)$. For the transport, therefore, the appropriate boundary and initial conditions are:

$$-\theta D_{1j}\frac{\partial c}{\partial x_j} + u_1\theta c = F(t)c_0, \quad 0 \leqslant t \leqslant t_0,$$
$$-\theta D_{1j}\frac{\partial c}{\partial x_j} + u_1\theta c = 0, \quad t > t_0$$
$$x_1 = 0, \quad \rho_{21} \leqslant x_2 \leqslant \rho_{22}, \quad \rho_{31} \leqslant x_3 \leqslant \rho_{32}, \tag{7a}$$

$$-\theta D_{1j}\frac{\partial c}{\partial x_j} + u_1\theta c = 0, \quad x_1 = 0, \quad \rho_{21} \geqslant x_2 \geqslant \rho_{22}, \quad \rho_{31} \geqslant x_3 \geqslant \rho_{32}, \quad t > 0 \tag{7b}$$

$$-\theta D_{1j}\frac{\partial c}{\partial x_j} + u_1\theta c = 0, \quad x_1 = L_1, \quad 0 \leqslant x_2 \leqslant L_2, \quad 0 \leqslant x_3 \leqslant L_3, \quad t > 0 \tag{7c}$$

$$-\theta D_{2j}\frac{\partial c}{\partial x_j}+u_2\theta c=0,\qquad x_2=0,\quad x_2=L_2,$$
$$0\leqslant x_1\leqslant L_1,\quad 0\leqslant x_3\leqslant L_3,\quad t>0 \tag{7d}$$

$$-\theta D_{3j}\frac{\partial c}{\partial x_j}+u_3\theta c=0,\quad x_3=0,\quad x_3=L_3,$$
$$0\leqslant x_1\leqslant L_1,\quad 0\leqslant x_2\leqslant L_2,\quad t>0 \tag{7e}$$

$$c=0,\quad 0\leqslant x_1\leqslant L_1,\quad 0\leqslant x_2\leqslant L_2,$$
$$0\leqslant x_3\leqslant L_3,\quad t=0. \tag{7f}$$

2.6. Implementation

We applied Eqs. (1) and (2), subject to (6a)–(6f) and Eqs. (7a)–(7f), respectively, to investigate the transport of a passive dissolved solute (chloride) in a combined vadose zone–groundwater flow system. The mixed form of Richards' equation governing 3-D water flow (Eq. (1)) was approximated by a fully implicit Euler scheme with a truncation error of $O(\Delta t,\Delta x_1^2,\Delta x_2^2,\Delta x_3^2)$. This scheme is convergent and unconditionally stable for the linear diffusion equation. The resulting system of nonlinear algebraic equations with respect to the pressure head, ψ is solved by iterative means, applying the so-called modified Picard method [7]. Picard (external) iterations are applied for both capillary and gravity terms, and the resulting system of linear algebraic equations is solved by line successive overrelaxation (LSOR) (inner) iterations [24].

For each time-step, Δt the CDE ((2)) governing solute transport in a 3-D flow domain was approximated by an operator-splitting approach [31,58]. Under this approach, during the first stage of computation, only the advective part of the equation is solved over the time interval Δt. During the second stage, the solution obtained in the first stage becomes the initial condition for solving a pure dispersion equation over the same Δt. A numerical solution of the advection equation was obtained by means of a second-order accurate, explicit finite difference scheme proposed by Zaidel and Levi [59], while dispersive fluxes were approximated by a standard central difference scheme. For more details, see the appendix in [49].

Solute transport was simulated for four different irrigation/rain intensities, $\mathrm{RI}(x_2,x_3)$. Assuming that $\mathrm{RI}(x_2,x_3)$ is log-normally distributed, values of $\mathrm{RI}(x_2,x_3)$ on each of the grid nodes at the soil surface were generated from $\mathrm{RI}(x_2,x_3)=\exp[\mu_{\log(\mathrm{RI})}+\sigma_{\log(\mathrm{RI})}R_N(x_2,x_3)$, where $\mu_{\log(\mathrm{RI})}$ and $\sigma_{\log(\mathrm{RI})}$ are the mean and the standard deviation of log(RI) and R_N is a random number taken from the normal distribution $N(0,1)$. The mean, $E[\mathrm{RI}]$ and the standard deviation, $\sigma[\mathrm{RI}]$ of the four rain/irrigation intensities were $E[\mathrm{RI}]=0.048$, 0.072, 0.120 and 0.240 m/d, and $\sigma[\mathrm{RI}]=0.016$, 0.024, 0.040 and 0.080 m/d, respectively. To match the behavior of actual rain/irrigation events, both the duration of such an event, $t_j''-t_j'$, and the time interval between successive events, $t_j'-t_{j-1}''$, were taken as time-dependent, ranging from 0.2 to 0.5 d and from 7 to 28 d, respectively. The same temporal distribution of $t_j''-t_j'$ and $t_j'-t_{j-1}''$ was adopted for the four different rain/irrigation intensities. Consequently, for a given elapsed time, t, the cumulative amounts of rain/irrigation water for $E[\mathrm{RI}]=0.072$, 0.120 and 0.240 m/d were equal to 1.5, 2.5 and 5 times, respectively, the cumulative amount of rain/irrigation water for $E[\mathrm{RI}]=0.048$ m/d.

It is important to separate between the effect of the rain/irrigation intensity and the effect of the cumulative amount of rain/irrigation on the response of the integrated flow domain. To do so, solute transport was simulated also for the high rain/irrigation intensity, i.e., $E[\mathrm{RI}]=0.240$ m/d and $\sigma[\mathrm{RI}]=0.080$ m/d, using a modified temporal distribution of $t_j''-t_j'$ and $t_j'-t_{j-1}''$. In this modification, the duration of each of the rain/irrigation events, $t_j''-t_j'$, was multiplied by a factor of 0.3, and the time interval between successive events, $t_j'-t_{j-1}''$, was changed accordingly. In other words, for a given elapsed time, the cumulative amount of rain/irrigation water associated with the latter case equaled the cumulative amount of rain/irrigation water associated with $E[\mathrm{RI}]=0.072$ m/d, $\sigma[\mathrm{RI}]=0.024$ m/d and the original temporal distribution of $t_j''-t_j'$ and $t_j'-t_{j-1}''$.

The movement of a chloride pulse was simulated for $L_1=12$ m, $L_2=25$ m, $L_3=10$ m, $\rho_{21}=5$ m, $\rho_{22}=15$ m, $\rho_{31}=1$ m and $\rho_{32}=9$ m, and $c_0=1$ kg/m^3. The total mass of solute entering the flow domain via the inlet zone at $x_1=0$ during a pulse of t_0, is given as

$$M_0\int_0^{t_0}\left[\int_{\rho_{21}}^{\rho_{22}}\int_{\rho_{31}}^{\rho_{32}}S_1(0,x_2,x_3,t)\,\mathrm{d}x_2\,\mathrm{d}x_3\right]\mathrm{d}t, \tag{8}$$

where the solute influx, s_1, is given as

$$s_1(0,x_2,x_3,t)=-\theta D_{11}\frac{\partial c}{\partial x_1}+u_1\theta c_0,\quad x_1=0,$$
$$\rho_{21}\leqslant x_2\leqslant\rho_{22},\quad \rho_{31}\leqslant x_3\leqslant\rho_{32}. \tag{9}$$

With $t_0=0.45$, 0.30, 0.18 and 0.09 d, for $E[\mathrm{RI}]=0.048$, 0.072, 0.12 and 0.24 m/d, respectively, M_0 was kept the same (1.3 kg) for all four cases. The flow and transport simulations proceeded until a solute breakthrough was completed at a vertical control plane (CP) located below the water table at the outlet ($x_2=L_2$). This occurred after 720, 550, 350 and 200 d for the four different rain/irrigation intensities, respectively. The respective cumulative amounts of rain/irrigation water were 1.20, 1.34, 1.43 and 1.64 m of water. Regarding the numerical solution statistics, the mean time step, Δt was $0.002d$ ($\Delta t_{\min}=0.0001d$ and $\Delta t_{\max}=0.01d$) while the average numbers of Picard external iterations and of LSOR inner iterations per time step, were 8 and 35, respectively.

3. Results and discussion

3.1. The velocity field

At the field scale, the movement and spreading of nonreactive solutes in the combined flow system are determined mainly by the velocity vector, $\underline{u}(\underline{x};t)$. In turn, $\underline{u}(\underline{x};t)$ is controlled by inherent properties of the formation (e.g., saturated hydraulic conductivity, and parameters which relate the unsaturated conductivity, K, to the water saturation, Θ), by flow-controlled attributes (e.g., pressure head, $\psi(\Theta)$), and by the boundary conditions imposed on the flow domain.

Vertical cross-sections (at $x_3 = 5$ m) of the 3-D velocity fields associated with the various rain/irrigation intensities before and after an irrigation event are depicted in Figs. 1 and 2, respectively, as patterns of arrows representing the velocity vectors. In these figures, the direction of the arrow is equal to the direction of the vector field at its base point, while the magnitude of the arrow is proportional to the magnitude of the vector field. During the redistribution stage (Fig. 1), a 3-D, rather complex velocity field is developed in the unsaturated zone. In this case the velocity fields associated with the different rain/irrigation intensities are quite similar. Notable is the upward flow in some locations in the upper part of the soil profile (Fig. 1). It stems from the inherent heterogeneity in the soil hydraulic properties and the change in the sign of the longitudinal component of the head gradient in the upper part of the soil profile as water content decreases. On the other hand, at the end of the infiltration stage (Fig. 2), the velocity fields associated with the different rain/irrigation intensities are quite different. After an irrigation/rain event, the flow in the upper part of the unsaturated zone is essentially unidirectional vertical, with small local deviations. Note that as the rain/irrigation intensity increases, the unidirectional vertical pattern of the velocity field persists to a larger soil depth (Fig. 2).

The cumulative probability plots of the components of the velocity vector $\underline{u} = (u_1, u_2, u_3)$ at the water table, $x_1 = \zeta(x_2, x_3)$, (Fig. 3), provide additional insight into the effect of the conditions at the soil surface on the velocity field. Fig. 3 shows that the effect of the recharge at the soil surface on the velocity, particularly on its vertical component, u_1, is significant during and immediately after a rain/irrigation event (Figs. 3(a), (c) and (e)) and may persist to relatively large vertical distances ($x_1 = 6$ m). On the other hand, during extended redistribution periods, the velocity is essentially insensitive to the recharge at the soil surface (Figs. 3(b), (d) and (f)).

The mean and standard deviation of $u_1(\underline{x})$, obtained by averaging $u_1(\underline{x})$ at the water table ($x_1 = \zeta(x_3, x_3)$), over the transverse direction, ($0 \leqslant x_3 \leqslant L_3$), and those of $u_2(\underline{x})$, obtained by averaging $u_2(\underline{x})$ over the vertical x_1x_3-plane in the saturated zone (i.e., $\zeta(x_2, x_3) \leqslant x_1 \leqslant L_1$, $0 \leqslant x_3 \leqslant L_3$)), as functions of x_2 are depicted in Fig. 4. As expected, the mean of the vertical component of the velocity $\langle u_1(x_2; x_1 = \zeta, t)\rangle$ (Fig. 4(a)) increases with increasing recharge at the soil surface. On the other hand, the respective standard deviations (Fig. 4(b)) are quite similar. The positive recharge from the unsaturated zone (i.e., $u_1(x_2; x_1 = \zeta, t) > 0$) resulted in a nonuniform mean flow in the saturated zone, i.e., the mean velocity in the saturated zone, $\langle u_2(x_2; t)\rangle$ (Fig. 4(c)) varies linearly in the x_2 direction as $\langle u_2(x_2; t)\rangle = [1 + \beta(x_2 - x_0)]\langle u_2(x_2 = x_0; t)\rangle$, in which $x_0 = 0$. Application of a linear regression analysis to the simulated data of $\langle u_2(x_2; t)\rangle$ yields $\beta = 0.00347$, 0.00467, 0.00529 and 0.00748 m^{-1} (and coefficients of determination,

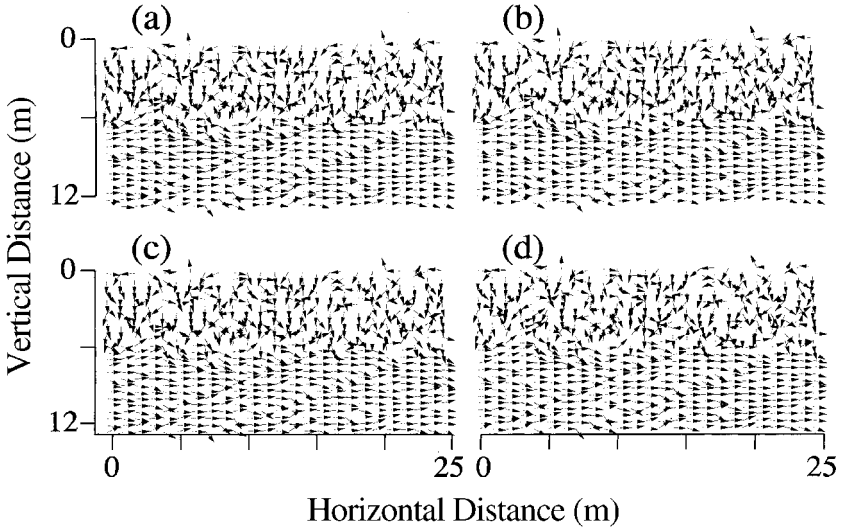

Fig. 1. Velocity fields in the vertical x_1x_2-plane at $x_3 = 10$ m, just before a rain/irrigation event for four different recharge rates at the soil surface: IR = 0.048 m/d (a); IR = 0.072 m/d (b); IR = 0.120 m/d (c); and IR = 0.240 m/d (d).

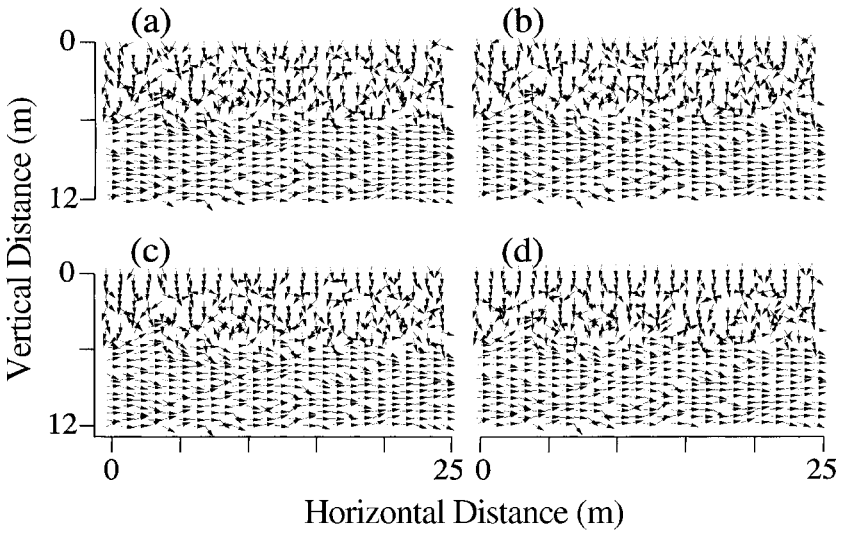

Fig. 2. Velocity fields in the vertical x_1 x_2-plane at $x_3 = 10$ m, just after a rain/irrigation event for four different recharge rates at the soil surface: IR = 0.048 m/d (a); IR = 0.072 m/d (b); IR = 0.120 m/d (c); and IR = 0.240 m/d (d).

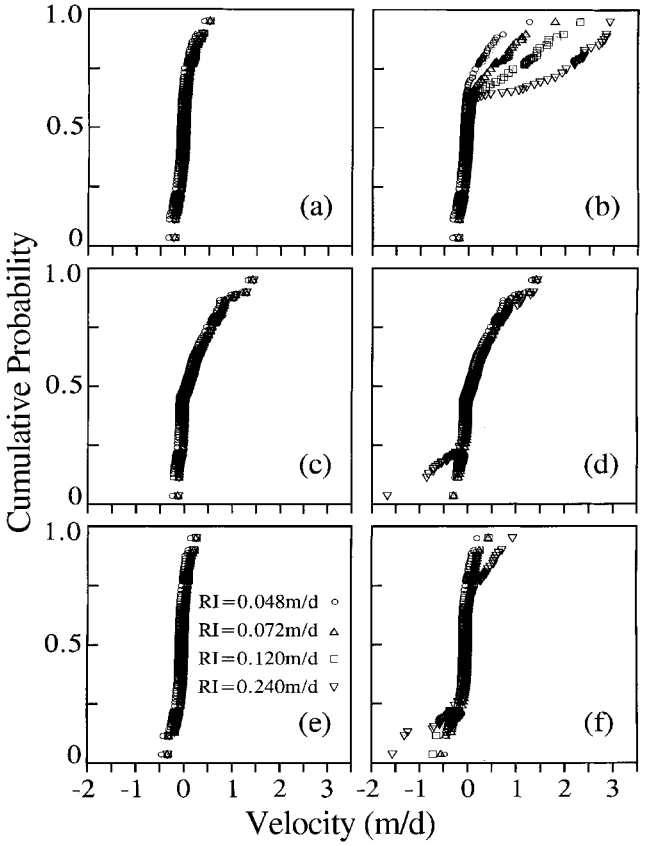

Fig. 3. Cumulative probability plots of u_1 (a), (b), u_2 (c), (d), and u_3 (e), (f) at the water table ($x_1 = \zeta(x_2, x_3)$), associated with the different recharge rates at the soil surface. Note that (a), (c) and (e) correspond to the time just before an irrigation, while (b), (d) and (f) correspond to the time at which the irrigation ceases.

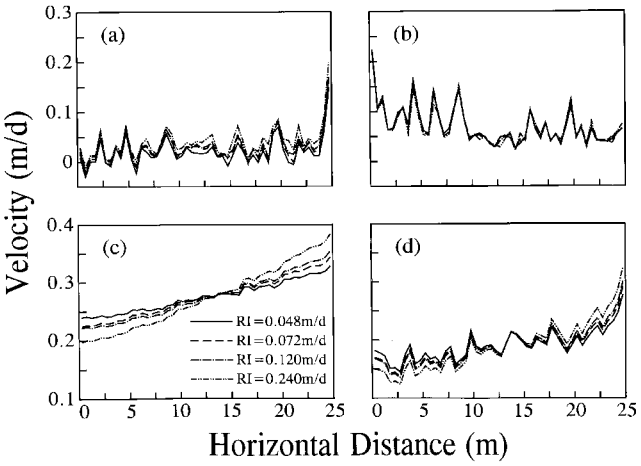

Fig. 4. Mean (a) and standard deviation (c) of u_1 at the water table ($x_1 = \zeta(x_2, x_3)$) obtained by averaging u_1 along the x_3-axis, and mean (b) and standard deviation (d) of u_2, obtained by averaging u_2 over the vertical x_1x_3-plane in the saturated zone, associated with the four different recharge rates, as functions of horizontal distance.

$r^2 = 0.977$, 0.987, 0.981 and 0.985), for $E[\mathrm{RI}] = 0.048$, 0.072, 0.120 and 0.240 m/d, respectively. Fig. 4(c) clearly demonstrates that the degree of nonuniformity in the mean flow in the saturated zone increases with increasing recharge at the soil surface.

Figs. 1–4 clearly demonstrate the effect of the recharge at the soil surface on the velocity field of the combined flow system. The implications for transport will be discussed in the following sections.

3.2. Displacement and spreading of solute concentration

The solute-spreading associated with the various recharges at the soil surface are illustrated in Fig. 5. This figure displays contour lines of the simulated solute resident concentrations, c, in the vertical cross-section of the heterogeneous soil (located at $x_3 = 5$ m), obtained

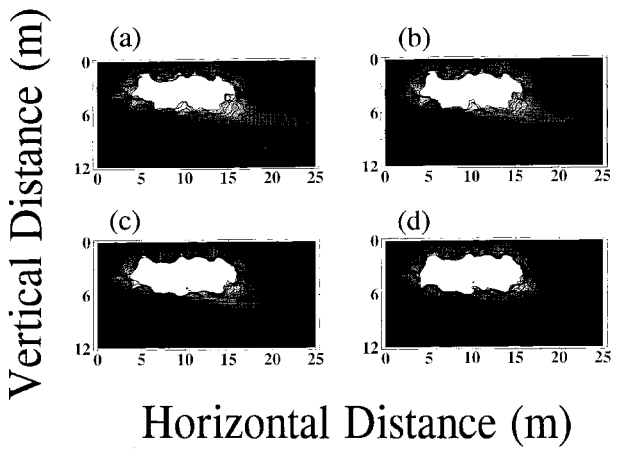

Fig. 5. Contours of the simulated solute concentrations in a vertical x_1 x_2-plane at $x_3 = 10$ m, associated with four different recharge rates at the soil surface: IR = 0.048 m/d (a); IR = 0.072 m/d (b); IR = 0.120 m/d (c); and IR = 0.240 m/d (d). Results are depicted for travel distance of $R_1 = 4$ m. The darkest shaded contour corresponds to 0.05 of mean concentration, $\langle c(\underline{x};t)\rangle$, and contour increment is $0.10\langle c(\underline{x};t)\rangle$.

from the solution of (1) subject to (6a)–(6f) and the solution of (2) subject to (7a)–(7f). Note that the center of mass of each of the plumes in Fig. 5 has traveled a vertical distance of 4 m. The irregular, ostensibly erratic, spatial variation of c shown in Fig. 5 is attributed to the small-scale variability in the hydraulic properties of the heterogeneous formation. For a given displacement of the plume's center of mass, the plume spreading in the vertical direction, and, concurrently, the penetration of the plume into the groundwater increase with decreasing recharge at the soil surface. When the plume invades the groundwater (Figs. 5(a) and (b)), it exhibits a significant spreading in the horizontal direction along the x_2-axis, with its accompanying dilution. As was shown in earlier analyses [41,49,50], the greater solute spreading in the unsaturated zone associated with decreasing recharge at the soil surface, stems from the decrease in water saturation and, concurrently, the increase in the relative variability in the response of the flow domain, as the recharge at the soil surface decreases.

The solute plumes in Fig. 5 are quantified here in terms of the spatial moments of the distribution of the solute resident concentration, c given [13] as

$$M(t) = \int \theta(\underline{x},t)c(\underline{x},t)\,\mathrm{d}\underline{x}, \tag{10a}$$

$$\underline{R}\,(t) = \frac{1}{M}\int \theta(\underline{x},t)c(\underline{x},t)\underline{x}\,\mathrm{d}\underline{x}, \tag{10b}$$

$$S'_{ij}(t) = \frac{1}{M}\int \theta(\underline{x},t)c(\underline{x},t)[x_i - R_i(t)]\,[x_j - R_j(t)]\,\mathrm{d}\underline{x}, \tag{10c}$$

where M is the total mass of solute, $\underline{R}(t) = (R_1, R_2, R_3)$ the coordinate of the centroid of the solute plume, and $S'_{ij}(t)$ $(i,j = 1,2,3)$ are second spatial moments, proportional to the moments of inertia of the plume.

Note that under ergodic conditions for the spatial moments, assumed to prevail if the lateral extent of the entry zone is large enough, as compared with the scale of the formation heterogeneity in the horizontal direction, $S_{ij}(t) = S'_{ij}(t) - S'_{ij}(0) \approx X_{ij}(t,0)$, where $X_{ij}(t;0)$ $(i,j = 1,2,3)$ is the one-particle displacement covariance. Hence, under these conditions, the one-particle-trajectory statistical moments characterize the spatial moments of the solute plume.

The dependence of the longitudinal, R_1, and transverse, R_i $(i = 2,3)$ components of the coordinate of the centroid of the solute plume, $\underline{R}$, upon time, t, until a solute discharge has been started at the outlet of the flow domain (located at $x_2 = L_2$, $0 \leqslant x_3 \leqslant L_3$, $\zeta(x_2,x_3) \leqslant x_1 \leqslant L_1$), is depicted in Fig. 6. As expected, the center of mass is displaced vertically in the direction of the mean flow, in a manner which is related to the recharge at the soil surface. The time fluctuations in R_1 (Fig. 6), originating from the recharge cycles at the soil surface increase with increasing recharge at the soil surface. They are

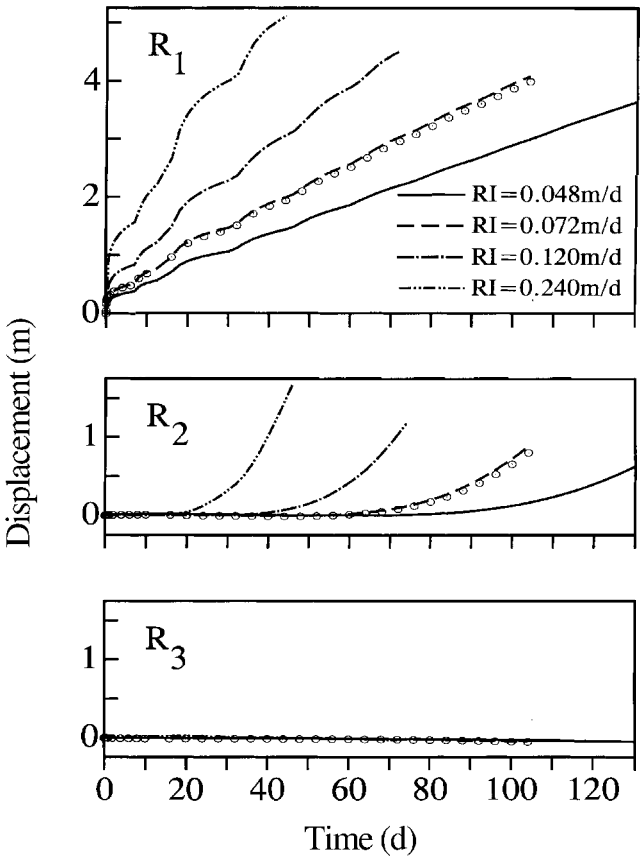

Fig. 6. Longitudinal (R_1) and transverse (R_2 and R_3) components of the coordinate location of the solute center of mass (see (10b)) as functions of elapsed time, t, for four different recharge rates. Open circles denote results for RI = 0.240 m/d and the modified temporal distribution of the rain/irrigation cycles.

smoothed out as time elapses and the center of mass of the plume is displaced to a sufficiently large vertical distance from the soil surface.

As time elapses and the solute plume invades the groundwater, the center of mass of the plume is shifted towards the direction of the mean head gradient along the x_2-axis. Because the mean velocity in the saturated zone, $\langle u_2(x_2;t)\rangle$ (Fig. 4(c)) varies linearly in the x_2 direction, R_2 increases with time at a rate faster than linearly in t. Note that the change of R_2 with time increases with increasing recharge at the soil surface, while R_3 is essentially time-invariant, independent of the recharge at the soil surface.

Estimated values of the longitudinal, S_{11} and the transverse, S_{22} and S_{33} components of the spatial covariance tensor, $S_{ij}(t) = S'_{ij}(t) - S'_{ij}(0)$ $(i,j = 1,2,3)$ as functions of the travel distance of the center of mass, R_1, are given in Fig. 7. Since the spatial covariance of the solute distribution is a measure of the spreading of the distribution about its center of mass, the changes in the covariance structure with travel distance may reflect the changes of the concentration distribution that occur because of the heterogeneity induced in the solute velocity field by small-scale heterogeneity in the soil hydraulic properties. For a given recharge at the soil surface, the longitudinal component, S_{11}, depicted in Fig. 7, generally describes a transport process which is initially controlled by convection only (i.e., S_{11} is initially proportional to the square of the travel distance), and is then continuously changed to a convection–dispersion transport process (for which S_{11} increases linearly with travel distance). The fluctuations in S_{11} stem from the fluctuations in the downward displacement of the center of mass (Fig. 6), which, in turn, stem from the temporal variations of the recharge at the soil surface. The transverse components, S_{22} and S_{33}, however, fluctuate only slightly in time and do not approach the constant asymptotic values which characterize the convection–dispersion transport process when the mean head gradient coincides with the longitudinal axis of the formation heterogeneity [13]. Instead, the evolution of S_{22} and S_{33} at a rate faster than linearly in R_1, persists over longer travel distances, and their magnitudes are only slightly smaller than that of S_{11}. As the leading edge of the solute plume invades the groundwater and R_2 increases with time (Fig. 6), S_{22} increases rapidly with travel distance and its magnitude considerably exceeds that of S_{11}.

The relatively small disparity between the magnitudes of the longitudinal and the transverse components of the displacement covariance (Fig. 7) stems from the multi-dimensionality of the flow variation (Figs. 1 and 2), and the resulting relatively small discrepancy between the magnitudes of the longitudinal and the transverse components of the velocity variance. During redistribution periods, which, in turn, dominate the rain/irrigation cycles, the ratio between the transverse and the longitudinal components of the velocity variance, $R_{vv} = \langle u_i'^2\rangle/\langle u_1'^2\rangle$ $(i = 2,3)$ in the unsaturated region may approach unity throughout most of this region. The relatively large value of R_{vv} in the unsaturated zone is shown to increase the lateral mixing of the solute, effectively smoothing out the extremes in solute convection, to slow down the plume spreading in the longitudinal direction and, at the same time, to accelerate its spreading in the transverse directions.

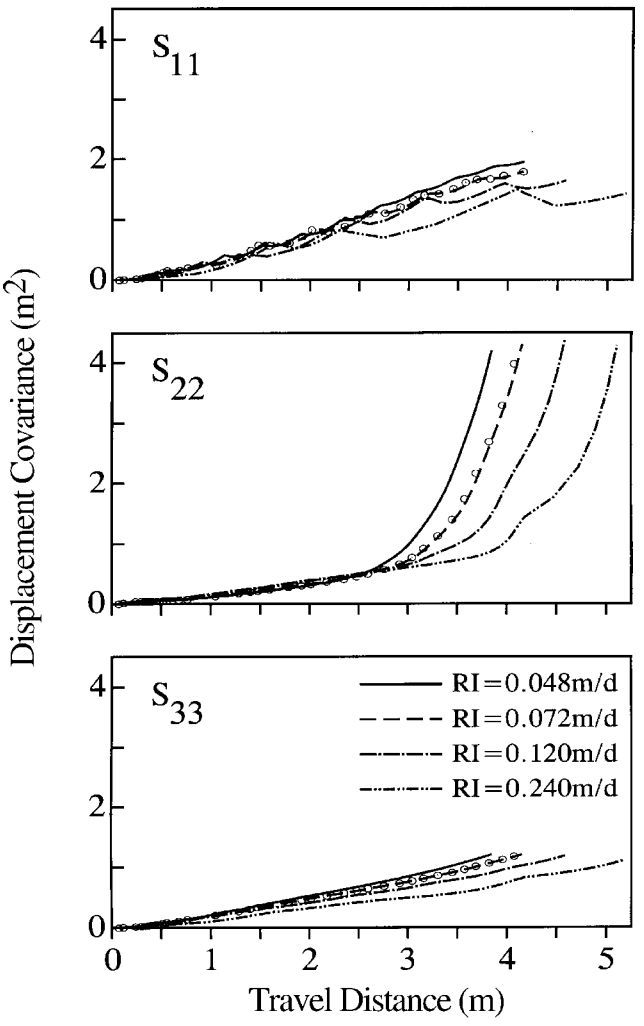

Fig. 7. Longitudinal (S_{11}) and transverse (S_{22} and S_{33}) components of the spatial covariance tensor (see (10c)) as functions of travel distance, for four different recharge rates. Open circles denote results for RI = 0.240 m/d and the modified temporal distribution of the rain/irrigation cycles.

For a given displacement of the solute plume's center of mass, the spreading of the plume increases with decreasing recharge at the soil surface, and, concurrently, with decreasing degree of saturation in the unsaturated zone. This result is in qualitative agreement with the results of first-order analysis of transport under steady-state unsaturated flow [41], and numerical

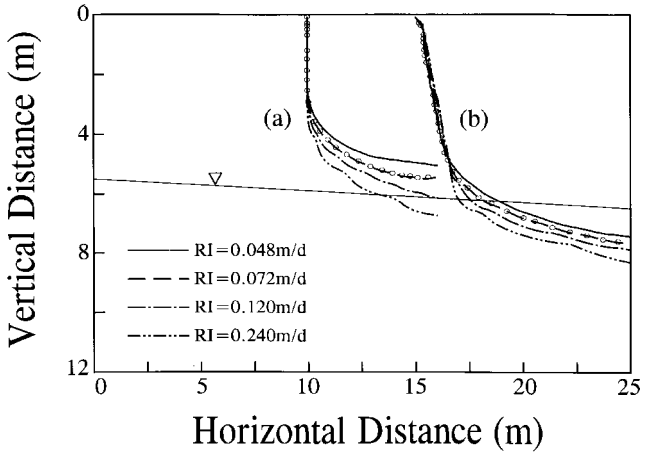

Fig. 8. Trajectories of the centers of mass of the solute plumes (a), and trajectories of the downstream boundary of the solute plumes (b), in the vertical x_1x_2-plane, associated with four different recharge rates. Open circles denote results for RI = 0.240 m/d and the modified temporal distribution of the rain/irrigation cycles.

simulations of transport under transient, unsaturated flow [49,50].

Fig. 8 presents trajectories of the center of mass of the solute plumes, and trajectories of the downstream boundary of the solute plumes in the vertical x_1x_2-plane, associated with the different recharge rates. It is shown in Fig. 8(a) that the soil depth at which the trajectories of the center of mass of the solute plume start to deflect from the vertical x_1-axis, increases with increasing recharge at the soil surface. On the other hand, the transverse crossing point of the downstream boundary of the solute plume and the water table (Fig. 8(b)) decreases with increasing recharge at the soil surface. These results stem from the fact that in the unsaturated zone, the disparity between the magnitude of the vertical component of the velocity vector, u_1 and the magnitudes of its horizontal components, u_2 and u_3, increases with increasing recharge at the soil surface (Fig. 3).

3.3. Solute breakthrough

Solute breakthrough is calculated from the flux-averaged concentration, c_f, defined [32] by $c_f = \int \underline{s} \cdot \underline{v}\, dA / \int \theta \underline{u} \cdot \underline{v}\, dA$, where $\underline{s}$ and $\underline{u}$ are the solute flux and the velocity vectors, respectively, with $\underline{s} = \underline{s} \cdot \underline{v}$ and $\theta \underline{u} = \theta \underline{u} \cdot \underline{v}$ being the mass of solute and the volume of water per unit time and unit area moving through a surface element of unit normal v, and water saturation, θ and the integration is over a planar area A.

Mean solute breakthrough curves (BTCs) at an horizontal CP located at the water table ($x_1 = 6$ m), and at a vertical CP located below the water table at the outlet ($x_2 = 25$ m) are depicted in Figs. 9(a) and (b), respectively. The expected flux concentrations, $\langle c_f(t) \rangle$ in Fig. 9(a) were evaluated by averaging c_f over a time-dependent horizontal region defined by the lateral spreading of the solute plume in the CPs located at the water table ($x_1 = 6$ m). Similarly, the expected BTCs in Fig. 9(b) were obtained by averaging c_f over a vertical region defined by the vertical spreading of the solute plume in a given CP located below the water table at $x_2 = 25$ m ($x_2 = L_2$).

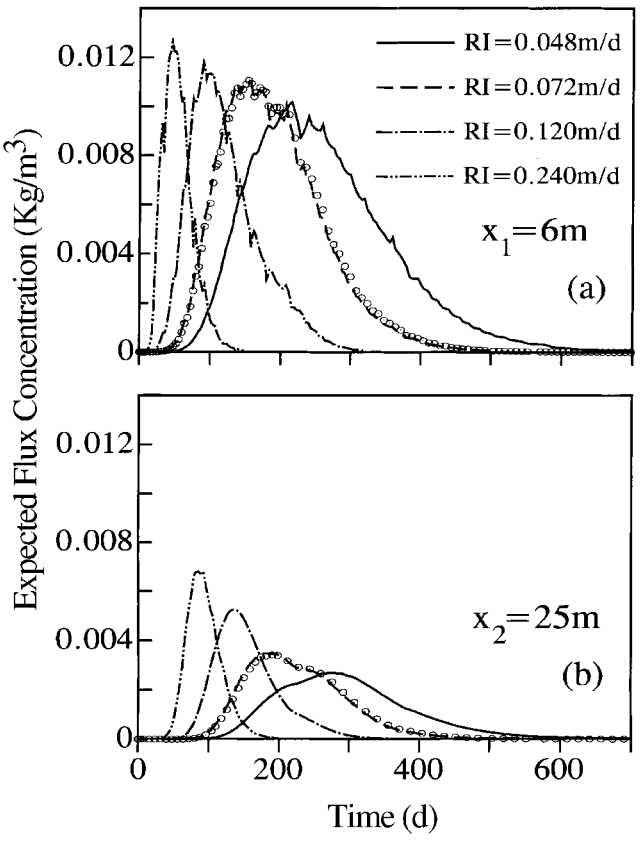

Fig. 9. Expected flux concentration crossing control planes located at $x_1 = 6$ m in the unsaturated region (a), and at $x_2 = 25$ m in the saturated region (b), as functions of elapsed time, for four different recharge rates. Open circles denote results for RI = 0.240 m/d and the modified temporal distribution of the rain/irrigation cycles.

The effect of the recharge at the soil surface on the expected BTCs in both the unsaturated and the saturated regions is clearly demonstrated in Fig. 9. The expected solute BTCs exhibit larger peak, earlier peak arrival, and less spreading as the recharge at the soil surface increases. Notable are the smaller flux concentrations in the saturated region than in the unsaturated zone, due to subsequent spreading and dilution of the solute plume in the saturated region. Note also that the expected BTCs in the unsaturated region are more erratic than those in the saturated region. This is due to the more complex velocity field in the former region (Figs. 1 and 2).

The dimensionless BTCs, $\langle C(T,L) \rangle$, depicted in Fig. 10, provide further insight on the effect of the recharge at the soil surface on the solute breakthrough in both

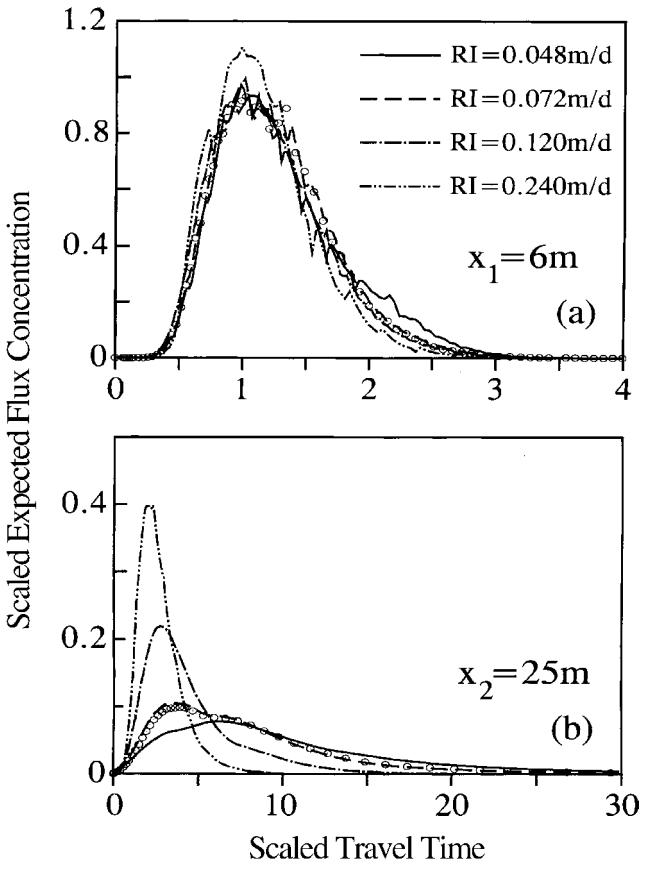

Fig. 10. Scaled expected flux concentration crossing control planes located at $x_1 = 6$ m in the unsaturated region (a), and at $x_2 = 25$ m in the saturated region (b), as functions of scaled travel time, for four different recharge rates. Open circles denote results for RI = 0.240 m/d and the modified temporal distribution of the rain/irrigation cycles.

regions. Here $\langle C(T;L\rangle = \langle c_f(T;L)\rangle / \int_0^\infty \langle c_f(T;L)\rangle \, dT$, $T = t\langle V_i\rangle/L$, L is the distance to the CP, and V_i $(i = 1,2)$ are the vertical and the horizontal (parallel to the x_2-axis) components, respectively, of the effective solute velocity vector, $\underline{V}$. The components of $\underline{V}$ are calculated as the time rate of change of the displacement of the solute plume center of mass, i.e.

$$\underline{V} = [dR_1/dt, dR_2/dt, dR_3/dt]^T. \quad (11)$$

Note that in the case of the unsaturated region, $L = x_1$. On the other hand, in the case of the saturated region, $L = x_2 - \chi$, where χ is the transverse crossing point of the down stream boundary of the solute plume and the water table (Fig. 8(b)).

The normalized BTCs at the bottom of the unsaturated region (Fig. 10(a)) exhibit slightly earlier solute peak arrival and less spreading as the recharge at the soil surface increases. These results are in qualitative agreement with the results of first-order analysis of transport under steady-state, unsaturated flow [41], and numerical simulations of transport under transient, unsaturated flow [49,50]. As was emphasized in the previous section, the results in Fig. 10(a) can be explained based on the effect of the recharge rate at the soil surface on water saturation, and, concurrently, on the relative variability in the response of the unsaturated flow domain.

The normalized BTCs in the saturated region (Fig. 10(b)) exhibit considerable skewness that is characterized by a delayed peak arrival, and by an exceedingly long tailing. The effect of the recharge at the soil surface, and, concurrently, of the groundwater recharge from the unsaturated zone (Fig. 4(a)) and the nonuniformity of the groundwater flow (Fig. 4(c)), on the solute BTCs at $x_2 = L_2$ is substantial. The expected solute BTCs exhibit larger peak, earlier peak arrival, and less spreading as the recharge at the soil surface increases. These results are in qualitative agreement with the results of the analytical study of Destouni and Graham [18]. Their results suggest that under nonuniform groundwater flow ($\beta > 0$), the resultant nonstationary travel time probability density function (PDF), exhibits shorter travel times and less spreading than a stationary travel time PDF associated with uniform groundwater flow ($\beta = 0$). In agreement with the results for the nonstationary travel time PDF, they found that the expected solute BTC exhibited earlier solute arrival and less spreading as β increased.

Figs. 5–10 show that characteristics of the transport associated with $E[\mathrm{RI}] = 0.072$ m/d, $\sigma[\mathrm{RI}] = 0.024$ m/d and the original temporal distribution of $t''_j - t'_j$ and $t'_j - t''_{j-1}$, and those associated with $E[\mathrm{RI}] = 0.240$ m/d, $\sigma[\mathrm{RI}] = 0.080$ m/d and the modified temporal distribution of $t''_j - t'_j$ and $t'_j - t''_{j-1}$, are almost indistinguishable. This suggests that for the case in which the solute plume is displaced to a sufficiently large vertical distance from the inlet zone at the soil surface, the variable that controls the transport is the cumulative recharge at the soil surface, $\mathrm{CR}(t) = \int_t F(t')\,dt'$ $(F(t) = RI, t' < t < t'', F(t) = 0,$ elsewhere), and not the recharge rate, RI. Note that unlike in steady-state, unsaturated flows in which $\mathrm{CR} = \mathrm{RI}t$, in transient, unsaturated flows originating from a periodic recharge at the soil surface, CR is a function of both RI and the temporal distribution of the duration of a rain/irrigation event, $t''_j - t'_j$, and the time interval between successive events, $t'_j - t''_{j-1}$.

4. Summary and concluding remarks

The main purpose of the present study was to investigate the field-scale transport of tracer solutes under realistic field conditions in a 3-D, heterogeneous, vdose zone-groundwater flow system. Detailed numerical simulations of the flow and the transport were employed in order to analyze solute spreading and breakthrough,

taking into account different recharge rates at the soil surface. The results of this investigation are represented in Figs. 1–10. The main findings of the present paper may be summarized as follows:

1. For given spatial heterogeneity in the formation properties, the pattern of velocity field, and, consequently, the spreading and the breakthrough of the solute pulse, are considerably affected by the recharge at the soil surface.
2. The realistic, periodic boundary conditions at the soil surface (i.e., $F(t) = \mathrm{RI}$, $t' < t < t''$, $F(t) = 0$, elsewhere), considered in this study, lead to periodicity in the response of the flow system which might persist to a relatively large soil depth.
3. Smaller recharge at the soil surface is shown to decrease the magnitude and persistence of the vertical component of the velocity field in the unsaturated zone. Consequently, smaller recharge at the soil surface leads to a decrease in both the groundwater recharge from the unsaturated zone and the degree of nonuniformity of the groundwater flow.
4. Smaller recharge at the soil surface is shown to increase both the longitudinal, and, especially, the transverse spreading of the solute plume, and to increase the skewing of the expected solute BTC in the unsaturated region. Furthermore, smaller recharge at the soil surface decreases the extent of the vertical penetration of the solute plume into the groundwater, delays peak arrival and considerably increases the spreading of the expected solute BTC in the saturated region.
5. For the combined flow system considered here in which the solute plume is displaced to a sufficiently large vertical distance from the inlet zone at the soil surface, the variable that controls the transport is the cumulative recharge at the soil surface, and not the recharge rate.

We would like to emphasize that the numerical experiments conducted in the present study provide detailed information on the consequences of spatial heterogeneity of the soil properties for the transport of solutes under quite realistic conditions. Such information cannot, in general, be obtained in practice from field investigations. We would like to stress, however, that the conclusions drawn from the present study should be considered with caution, in as much as the numerical results presented are based on analyses of single realizations of the formation properties. Results of recent analyses of transport under transient flow in a variably saturated, 3-D, heterogeneous formation [50], however, suggest that because of the relatively large lateral extent of the solute input zone, the simulated results might be sufficiently accurate to indicate appropriate trends.

Before concluding, we would like to stress that in our simulations we did not take into account the hysteresis in the local ψ–θ relations caused by contact angle, irregular geometry and nonwetting fluid (air) entrapment effects, nor hysteresis in the local K–θ relations caused by air entrapment effects. Using 1-D column experiments and simulations, Lenhard et al. [33] illustrated the importance of air entrapment and saturation hysteresis in the case of fluctuating water table conditions. On the other hand, using 1-D and 2-D simulations, Kaluarachchi and Parker [30] showed that both flux-controlled boundary conditions and heterogeneity in the formations properties may diminish the effects of hysteresis and air entrapment on infiltration and seepage. In as much as, in our simulations, water table fluctuations were negligibly small, we believe that the neglect of hysteresis in the local K–ψ–θ relations has only a small effect on the response of our heterogeneous, combined unsaturated–saturated flow system.

Acknowledgements

This is contribution 611/99, 1999 series, from the Agricultural Research Organization, the Volcani Center, Bet Dagan, Israel. This research was supported in part by a grant from the United States–Israel Binational Science Foundation (BSF).

References

[1] Ababou R. Three-dimensional flow in random porous media. Ph. D. thesis, Mass Inst of Technol, Cambridge, MA, 1988.
[2] Amoozegar-Fard A, Nielsen DR, Warrick AW. Soil solute concentration distribution for spatially varying pore water velocities and apparent diffusion coefficients. Soil Sci Soc Am J 1982;46:3–8.
[3] Bear J. Dynamics of fluids in porous media. New York: Elsevier; 1972.
[4] Bresler E, Dagan G. Unsaturated flow in spatially variable fields. 3. Solute transport models and their application to two fields. Water Resour Res 1983;9:429–35.
[5] Butters GL, Jury WA, Ernst FF. Field scale transport of bromide in an unsaturated soil. 1. Experimental methodology and results. Water Resour Res 1989;25:1575–81.
[6] Byers E, Stephans DB. Statistical and stochastic analyses of hydraulic conductivity and particle-size in a fluvial sand. Soil Sci Soc Am J 1983;47:1072–81.
[7] Celia M, Bouloutas E, Zarba R. A general mass-conservative numerical solution of the unsaturated flow equation. Water Resour Res 1990;26:1483–96.
[8] Cvetkovic V, Shapiro AM, Dagan G. A solute flux approach to transport in heterogeneous formation. 2. Uncertainty analysis. Water Resour Res 1992;28:1377–88.
[9] Dagan G. Stochastic modeling of groundwater flow by unconditional and conditional probabilities. 2. The solute transport. Water Resour Res 1982;18:835–48.
[10] Dagan G. Solute transport in heterogeneous porous formations. J Fluid Mech 1984;145:151–77.
[11] Dagan G. Statistical theory of groundwater flow and transport: pore to laboratory laboratory to formation and formation to regional scale. Water Resour Res 1986;22:120S–34S.

[12] Dagan G. Time-dependent macrodispersion for solute transport in anisotropic heterogeneous aquifers. Water Resour Res 1988;24:1491–500.
[13] Dagan G. Flow and transport in porous formations. Berlin: Springer; 1989.
[14] Dagan G, Bresler E. Solute transport in unsaturated heterogeneous soil at field scale. 1. Theory. Soil Sci Soc Am J 1979;43: 46l–7.
[15] Dagan G, Cvetkovic V, Shapiro AM. A solute flux approach to transport in heterogeneous formations. 1. The general framework. Water Resour Res 1992;28:1369–76.
[16] Destouni G, Cvetkovic V. The effect of heterogeneity on large scale solute transport in the unsaturated zone. Nordic Hydrol 1989;20:43–52.
[17] Destouni G, Cvetkovic V. Field scale mass arrival of sorptive solute into the groundwater. Water Resour Res 1991;27:1315–25.
[18] Destouni G, Graham W. Solute transport through an integrated heterogeneous soil-groundwater system. Water Resour Res 1995;31:1935–44.
[19] Ellsworth TR, Jury WA, Ernst FF, Shouse PJ. A three-dimensional field study of solute transport through unsaturated layered porous media. 1. Methodology, mass recovery and mean transport. Water Resour Res 1991;27:951–65.
[20] Freyberg DL. A natural gradient experiment on solute transport in a sand aquifer. 1. Spatial moments and the advection and dispersion of nonreactive tracers. Water Resour Res 1986;22:2031–46.
[21] Garabedian SP, LeBlanc DR, Gelhar LW, Celia MA. Large-scale natural gradient tracer test in sand and gravel, Cape Cod Massachusetts. 1. Analysis of spatial moments for a nonreactive tracer. Water Resour Res 1992;27:911–24.
[22] Gelhar LW. Stochastic subsurface hydrology from theory to applications. Water Resour Res 1986;22:135S–45S.
[23] Gelhar LW, Axness C. Three-dimensional stochastic analysis of macrodispersion in aquifers. Water Resour Res 1983;19:161–90.
[24] Hageman LA, Young DM. Applied iterative methods. New York: Academic Press; 1981.
[25] Hess KM, Wolf SH, Celia MA. Large-scale natural gradient tracer test in sand and gravel, Cape Cod, Massachusetts. 3. Hydraulic conductivity variability and calculated macrodispersivities. Water Resour Res 1992;28:2011–7.
[26] Hoeksema RJ, Kitanidis PK. An application of the geostatistical approach to the inverse problem in two-dimensional groundwater modeling. Water Resour Res 1984;20:1009–20.
[27] Jones AJ, Wagenet RJ. In-situ estimation of hydraulic conductivity using simplified methods. Water Resour Res 1984;20: 1620–6.
[28] Jury WA. Simulation of solute transport using a transfer function model. Water Resour Res 1982;18:363–8.
[29] Jury WA, Sposito G. Field calibration and validation of solute transport models for the unsaturated zone. Soil Sci Soc Am J 1985;49:1331–441.
[30] Kaluarachchi JJ, Parker JC. Effects of hysteresis with air entrapment on water flow in the unsaturated zone. Water Resour Res 1987;23:1967–76.
[31] Konikow LF, Bredehoeft JD. Computer models of two-dimensional solute transport in groundwater. In: Techniques of water-resources investigations of the US Geological Survey, US Gov. Print. Off., Washington, DC, 1978 [Chapter C2].
[32] Kreft A, Zuber A. On the physical meaning of the dispersion equation and its solution for different initial and boundary conditions. Chem Eng Sci 1978;33:1471–80.
[33] Lenhard RJ, Parker JC, Kaluarachchi JJ. Comparing simulated and experimental hysteretic two-phase transient fluid flow phenomena. Water Resour Res 1991;27:2113–24.
[34] Moltyaner GL, Wallis CA. Characterization of aquifer heterogeneity by in situ sensing. Water Resour Res 1993;29:3417–31.
[35] Neuman SP, Winter CL, Newman CN. Stochastic theory of field-scale Fickian dispersion in anisotropic porous media. Water Resour Res 1987;23:453–66.
[36] Nielsen DR, Biggar JW, Erh KT. Spatial variability of field-measured soil-water properties. Hilgardia 1973;42:215–60.
[37] Polmann DJ, Mclaughlin D, Luis S, Gelhar LW, Ababou R. Stochastic modeling of large-scale flow in heterogeneous unsaturated soils. Water Resour Res 1991;27:1447–58.
[38] Roth K, Hammel K. Transport of conservative chemical through an unsaturated two-dimensional Miller-similar medium with steady state flow. Water Resour Res 1996;32:1653–63.
[39] Roth K, Jury AW, Fluhler H, Attinger W. Transport of chloride through an unsaturated field soil. Water Resour Res 1991;27:2533–41.
[40] Russo D. Stochastic analysis of vadose-zone solute transport in a vertical cross-section of heterogeneous soil during nonsteady water flow. Water Resour Res 1991;27:267–83.
[41] Russo D. Stochastic modeling of macrodispersion for solute transport in a heterogeneous unsaturated porous formation. Water Resour Res 1993a;29:383–97.
[42] Russo D. Stochastic modeling of solute flux in a heterogeneous partially saturated porous formation. Water Resour Res 1993b;29:1731–44.
[43] Russo D. On the velocity covariance and transport modeling in heterogeneous anisotropic porous formations. 2. Unsaturated flow. Water Resour Res 1995a;31:139–45.
[44] Russo D. Stochastic analysis of the velocity covariance and the displacement covariance tensors in partially saturated heterogeneous anisotropic porous formations. Water Resour Res 1995b;31:1647–58.
[45] Russo D. Stochastic analysis of flow and transport in unsaturated heterogeneous porous formation: effects of variability in water saturation. Water Resour Res 1998;34:569–81.
[46] Russo D, Bouton M. Statistical analysis of spatial variability in unsaturated flow parameters. Water Resour Res 1992;28:1911–25.
[47] Russo D, Bresler E. Soil hydraulic properties as stochastic processes: I. An analysis of field spatial variability. Soil Sci Soc Am J 1981;45:682–7.
[48] Russo D, Russo I, Laufer A. On the spatial variability of parameters of the unsaturated hydraulic conductivity. Water Resour Res 1997;33:946–56.
[49] Russo D, Zaidel J, Laufer A. Stochastic analysis of solute transport in partially saturated heterogeneous soil: I. Numerical experiments. Water Resour Res 1994;30:769–79.
[50] Russo D, Zaidel J, Laufer A. Numerical analysis of flow and transport in a three-dimensional partially saturated heterogeneous soil. Water Resour Res 1998;34:1451–68.
[51] Schulin R, van Genuchten MTh, Fluhler H, Ferlin P. An experimental study of solute transport in a stony field soil. Water Resour Res 1987;23:1785–94.
[52] Simmons CS. A stochastic–convective transport representation of dispersion in one-dimensional porous media systems. Water Resour Res 1982;18:1193–214.
[53] Sposito G, Jury WA, Gupta VK. Fundamental problems in the stochastic convection–dispersion model of solute transport in aquifers and field soils. Water Resour Res 1986;22:77–88.
[54] Sudicky EA. A natural gradient experiment on solute transport in a sand aquifer: spatial variability of hydraulic conductivity and its role in the dispersion process. Water Resour Res 1986;22:2069–82.
[55] Tompson AFB, Ababou R, Gelhar LW. Implementation of the three-dimensional turning bands random field generator. Water Resour Res 1989;25:2227–43.
[56] Tseng PH, Jury WA. Comparison of transfer function and deterministic modeling of area-average solute transport in heterogeneous field. Water Resour Res 1994;30:2051–64.

[57] van Genuchten MTh. A closed-form equation for predicting the hydraulic conductivity of unsaturated soils. Soil Sci Soc Am J 1980;44:892–8.

[58] Wheeler MF, Dawson CN. An operator splitting method for advection–diffusion–reaction problems. Tech. Rep. 87-9, Department of Mathematical Science, Rice University, Houston, Texas, May 1987.

[59] Zaidel JM, Levi BI. Numerical schemes for the solution of two-phase, three-component flow and transport in porous medium equations, Numerical Methods of Continuum Mechanics. 1980;11(5):75–89 [in Russian].

[60] Zaidel J, Russo D. Estimation of finite difference interblock conductivities for infiltration into initially dry soils. Water Resour Res 1992;28:2285–95.